776–790 *Nucleic Acids Research, 2021, Vol. 49, No. 2* *Published online 18 December 2020*
doi: 10.1093/nar/gkaa1227

The nucleoid-associated protein IHF acts as a 'transcriptional domainin' protein coordinating the bacterial virulence traits with global transcription

Sylvie Reverchon[1], Sam Meyer[1], Raphaël Forquet[1], Florence Hommais[1], Georgi Muskhelishvili[2,*] and William Nasser[1,*]

[1]Univ Lyon, Université Claude Bernard Lyon 1, INSA-Lyon, CNRS, UMR5240 MAP, F-69622, France and [2]Agricultural University of Georgia, School of Natural Sciences, 0159 Tbilisi, Georgia

Received November 12, 2020; Revised November 30, 2020; Editorial Decision December 03, 2020; Accepted December 07, 2020

ABSTRACT

Bacterial pathogenic growth requires a swift coordination of pathogenicity function with various kinds of environmental stress encountered in the course of host infection. Among the factors critical for bacterial adaptation are changes of DNA topology and binding effects of nucleoid-associated proteins transducing the environmental signals to the chromosome and coordinating the global transcriptional response to stress. In this study, we use the model phytopathogen *Dickeya dadantii* to analyse the organisation of transcription by the nucleoid-associated heterodimeric protein IHF. We inactivated the IHFα subunit of IHF thus precluding the IHFαβ heterodimer formation and determined both phenotypic effects of *ihfA* mutation on *D. dadantii* virulence and the transcriptional response under various conditions of growth. We show that *ihfA* mutation reorganises the genomic expression by modulating the distribution of chromosomal DNA supercoils at different length scales, thus affecting many virulence genes involved in both symptomatic and asymptomatic phases of infection, including those required for pectin catabolism. Altogether, we propose that IHF heterodimer is a 'transcriptional domainin' protein, the lack of which impairs the spatiotemporal organisation of transcriptional stress-response domains harbouring various virulence traits, thus abrogating the pathogenicity of *D. dadantii*.

INTRODUCTION

Plant–pathogen interaction is a multifaceted process, where molecules secreted by pathogens determine both their virulence as well as success in colonizing the host. Besides having limited access to nutrients and specific oligoelements, the pathogen must cope with numerous specific challenges including exposure to various types of stress and host defence reactions. The expression of virulence and adaptive traits must therefore be tightly coordinated to ensure efficient infection.

Among the plant-pathogenic *Dickeya* species causing soft-rot disease in a wide range of hosts, one of the widely used model organisms is *D. dadantii* (1). Studies of the invasion strategy of *D. dadantii* revealed a complex regulation combining utilization of the core metabolism and general stress-response genes with the sets of genes specifically responding to each encountered stress (2,3). This sophisticated genetic control mechanism is coordinated primarily at the level of transcriptional regulation of relevant genes involved in bacterial adaptation and virulence (4–8).

The bacterial adaptive response to stress involves alterations of chromosomal DNA topology modulated by abundant nucleoid-associated proteins (NAPs) that affect the expression of numerous genes, including the transcription factors (9,10). Changes in NAPs binding and chromosomal DNA supercoiling were shown to dynamically organise coherent domains of gene expression (aka CODOs) harbouring virulence traits, that emerge in particular constellations under conditions mimicking pathogenic growth (2,11–13). In *D. dadantii,* mutations inactivating either of the two highly abundant NAPs, FIS (Factor for Inversion Stimulation) or H-NS (Histone-like Nucleoid-Structuring protein), both modify the CODOs and strongly impair bacterial virulence (2,4,12,14).

IHF (Integration Host Factor), a NAP found in the phylum of Proteobacteria, is a heterodimer of IHFα and IHFβ proteins encoded by *ihfA* and *ihfB* genes, respectively, and one of the major bacterial NAPs with prominent capacity to induce sharp bends in the DNA (15). This capacity to change the local DNA trajectory underpins the assembly of various higher-order nucleoprotein structures

*To whom correspondence should be addressed. Tel: +33 4 72 43 85 68; Fax: +33 4 72 43 26 86; Email: William.nasser@insa-lyon.fr
Correspondence may also be addressed to Georgi Muskhelishvili. Email: g.muskhelishvili@icloud.com

and facilitates long-range interactions underlying the effect of IHF not only on gene transcription, but also on site-specific DNA recombination, replication, transposition and genome packaging (16–23). IHF was found to interact with a class of bacterial repetitive DNA elements located at the 3′ end of transcription units and was proposed to modulate gyrase binding and activity (24). However, while the crosstalk between other NAPs and DNA supercoiling has been analysed at the whole-genome scale (11,25), a comparable analysis is lacking for IHF.

The intracellular concentration of IHF changes during bacterial growth, increasing on transition of the cells to stationary phase (26). In *E. coli*, IHF appears to control numerous functions including metabolic, cell cycle and adaptive processes (27,28). In various *Salmonella* species IHF is shown to profoundly influence the expression of virulence genes, facilitate invasion associated with transition of bacterial cells to stationary phase (29) and promote biofilm formation (30). IHF activates the expression of virulence traits in human pathogens *Vibrio cholerae* (31) and *Vibrio fluvialis* (32) as well as in plant pathogens *Erwinia amylovora* (33) and *Dickeya zeae* (34). In the soil bacterium *Pseudomonas putida*, IHF activates the genes involved in adaptation to the post-exponential phase with limited effect on genes involved in central metabolism (35). In spite of this eminent role in bacterial pathogenicity, the mechanistic basis for the coordinating effect of IHF on the expression of virulence and adaptation traits remains unclear.

Previous studies revealed that in *D. dadantii* the IHF mutation leads to a growth defect and is more detrimental than in *E. coli* (36). However, the effect of IHF on *D. dadantii* virulence has not been explored so far and in plant pathogenic bacteria in general, the contribution of IHF to global gene expression remains obscure. In this study, by using a combination of phenotypic approaches with RNA Sequencing (RNA-seq) analysis, we characterize the effect of IHF on *D. dadantii* pathogenic growth and global gene expression. We show that *ihfA* mutation modulates the genomic distributions of DNA supercoiling, the organisation of CODOs, the preferences for lagging/leading strand usage and for local organisation of transcribed units causing massive reorganization of gene expression, including virulence genes required during both the symptomatic and asymptomatic phases of infection and thus, abrogates the pathogenic growth of *D. dadantii.*

MATERIALS AND METHODS

Bacterial strains and cell growth conditions

The bacterial strains used in this work are the *D. dadantii* strain 3937 isolated from Saintpaulia, its *ihfA* derivative (36), the *bcsA* mutant deficient in cellulose fiber production (37), the double *bcsA-ihfA* mutant obtained by generalized transduction using phage phiEC2 (38), the complemented *ihfA*/pEK strain. The pEK plasmid was generated by PCR using 3937 genomic DNA as template and the following primer couple: oligo ihf-Fw-BamHI (CC GGATCCGAATCGCCGTGATATTGCTGTGG), oligo ihf-Rev-PstI (CCCTGCAGTAATGCGGCCTTTTTGTC A). The PCR fragment was then cloned into the vector pBBR1-mcs4 between the BamHI and PstI restriction sites. In the resulting plasmid, *ihfA* is expressed under its own promoter.

All strains were grown at 30°C either in rich Luria broth (LB) medium or in M63 minimal salts medium (39) supplemented with a carbon source (polygalacturonate (PGA) at 0.2% (w/v) and sucrose or glycerol at 0.2% (w/v)). When required, antibiotics were used as follows: ampicillin (Ap), 100 μg mL^{-1}; novobiocin (Nov) 100 μg mL^{-1}. Liquid cultures were grown in a shaking incubator (220 rpm). Media were solidified by the addition of 1.5% agar (w/v).

Phenotype analyses

Detection of protease activity was performed on medium containing Skim Milk (12.5 g l^{-1}) and detection of cellulase activity was performed using the Congo red procedure (40). Detection of pectinase activity was performed on medium containing PGA using the copper acetate procedure as described by (41). Siderophore production was detected on chrome azurol S (CAS) agar plate. This assay is based on a competition for iron between the ferric complex of the dye CAS and siderophore (42). Semi-solid agar medium containing low concentration of agar (0.4% w/v) and standard agar plates containing carboxy-methyl cellulose (0.2% w/v) and glucose (0.2% w/v) were used to investigate the effect of the *ihfA* inactivation on the swimming and twitching motilities of *D. dadantii,* respectively.

For a visual assessment of cell aggregation, 5 ml of minimal M63 medium, supplemented with glycerol at 0.2% (v/v) was inoculated with an overnight culture grown in the same medium at a final density of 10^6 cells mL^{-1}. Bacteria were grown in water bath with low shaking (55 rpm) for 48 h. The planktonic cells were collected and the aggregate/biofilm structures were washed once with 2 ml of M63 medium. The aggregate/biofilm structures were then dissolved in 1–2 ml of M63 medium by pipetting up and down. Next, the free-living and sessile fractions were vortexed for 20 s and then the bacteria were estimated by measuring turbidity at 600 nm, given that an optical density at 600 nm (OD_{600}) of 1.0 corresponds to 10^9 bacteria ml^{-1}. Cells contained in aggregates were quantified versus the total number of cells contained in both aggregate and planktonic fractions for the different strains. Each value represents the mean of five different experiments and bars indicate the standard deviation.

Assay of pectate lyase was performed on toluenised cell extracts. Pectate lyase activity was determined by the degradation of PGA to unsaturated products that absorb at 235 nm (43) Specific activity is expressed as μmol of unsaturated products liberated min^{-1} mg^{-1} (dry weight) bacteria. Bacterial concentration was estimated by measuring turbidity at 600 nm, given that an optical density at 600 nm (OD_{600}) of 1.0 corresponds to 10^9 bacteria ml^{-1} and to 0.47 mg of bacteria (dry weight) ml^{-1}.

Pathogenicity assays were performed, as described in (44), with 5×10^6 bacteria in 5 μl of 50 mM KH_2PO_4 pH 7 buffer. Assays were carried out on one hundred chicory leaves for each strain. Negative controls were performed using sterile buffer. After a 24 h incubation period, the rotted tissues were collected and weighted.

Surproduction, purification of IHFαβ

The *ihfA* and *ihfB* genes were cloned in tandem under the T7 promoteur of plasmid pET20. Surproduction was performed in E. coli strain BL21-DE3 ΔihfA-ΔihfB after 0.8 mM IPTG induction for 3 h. Purification was achieved from 3 liters culture at OD_{600} nm 0.6. Bacterial cells were disrupted by French press. The clarified protein solution was submitted to ammonium sulfate precipitation and successive chromatography on heparin sepharose and sulphopropyl sepharose. At least 10 mg of purified IHF was obtained from the 3 liter culture.

Electrophoretic mobility shift assays (EMSA)

Probes for the assays were prepared by amplifications of DNA segments upstream of the encompassing the 5′ end of the open reading frame of the *pelD, cel5Z, acsF, hrpA, hrpL, hcpA, outC, thrA* and *proB* genes. Using the A of each translation start codon as a reference point (position +1), oligonucleotide primers amplified the +3 to −300 regions. The forward primers were fluorescently labelled in 5′ with FAME. Labeled probes were purified using PCR clean up Kit from Macherey Nagel. EMSA reactions contained 0–100 nM IHF protein, 100 ng of labeled probe and were performed in 20 μl of 10 mM Tris–HCl pH 8.0, 70 mM KCl, 10 mM $MgCl_2$, 1 mM DTT, 5% (v/v) glycerol, 100 μg/ml BSA, 200 ng poly dI.dC, 0.05% (v/v) nonidet P40. Protein–DNA binding reactions were carried out for 20 min at 30°C and then electrophoresed on a 4% DNA retardation gel with Tris-acetate pH 8 as running buffer. The apparent dissociation constants (Kd_{app}) were determined according to the method described by Carey (45). EMSA gels were subjected to densitometric analysis using Image Lab 6.0 software (Biorad). For each dilution of the IHF protein, amounts of free probe were determined and plotted against the IHF concentrations. The Kd_{app} constants correspond to the IHF concentrations at which half of the DNA probe is bound to the IHF protein.

Separation of plasmid topoisomers by gel electrophoresis

The multicopy plasmid pUC18 was extracted from *D. dadantii* WT strain and *ihfA* mutant by using the Qiaprep Spin Miniprep kit and 0.5–1 μg of plasmid DNA was electrophoresed on 1% agarose gel containing 2.5 μg ml^{-1} chloroquine. All electrophoresis was conducted in 20 cm long agarose gel with Tris–borate EDTA (TBE) as gel running buffer. The electrophoresis was run at 2.5 V cm^{-1} for 16 h. Under these conditions, topoisomers that are more negatively supercoiled migrate faster in the gel than more relaxed topoisomers. Chloroquine gels were subjected to densitometric analysis using Image Lab 6.0 software (Biorad). Distribution of topoisomers was analysed in each lane independently; the relative proportions of the different topoisomers of each lane were then compared with other lanes.

RNA extraction and transcriptomics data

The wild type (WT) strain and its *ihfA* derivative were used to analyse the global gene expression of cells grown under different conditions: M63 supplemented with 0.2% (w/v) sucrose as carbon source, with or without 0.2% (w/v) PGA. Cells were grown to the early exponential phase (OD_{600} = 0.2) and to the early stationary phase (OD_{600} = 0.9–1.2 for cells grown in M63/sucrose, and OD_{600} = 1.9–2.2 for cells grown in M63/sucrose/PGA medium). The different OD_{600} retained for the various culture media and strains correspond to a similar growth stage (i.e. transition from late exponential phase to early stationary phase), then aliquots were transferred to two flasks. One of them was kept as a control and the second was treated for 15 min with novobiocin to 100 μg l^{-1} final concentration. At this concentration, novobiocin has no impact on *D. dadantii* parental strain growth (14). For each condition, total RNAs were extracted using the frozen-phenol procedure (46). Control experiments for RNA extraction quality, absence of DNA contamination, and qRT-PCR validation of selected genes were conducted as previously (11). Further steps were carried out by Vertis Biotechnologie AG (http://www.vertis-biotech.com): rRNA depletion using the Illumina Ribo-Zero kit, RNA fragmentation, strand-specific cDNA library preparation, and Illumina NextSeq500 paired-end sequencing (∼15 million paired reads per sample). Transcriptomes were analysed as previously described (47) using softwares FastQC, Bowtie2 (reference genome NC 014500.1), and DESeq2 for differential expression. Significantly activated/repressed genes were selected with a threshold of 0.05 on the adjusted *P*-value.

Computational and statistical methods

The predicted binding sites of IHF were generated from its position weight matrix with Prodoric2 (48). Orientational distributions were analysed with a homemade Python code, where a gene/region is defined as convergent/divergent/tandem based on the orientation of the two neighbouring genes. Proportions were compared with chi-square tests. For genome-wide analyses, all parameters were computed over 500 kb scanning windows shifted by 4 kb, resulting in 1230 overlapping windows. The numbers of activated/repressed genes and of predicted binding sites in each window were transformed into z-scores by comparison to the null hypothesis of a homogeneous distribution of the considered quantity over the chromosome. In particular, in the inner wheels of Figure 11, a *z*-score >2 (resp. <2), depicted in red (resp. blue), indicates a statistically significant enrichment of the 500 kb region in up-regulated (resp. down-regulated) genes among differentially expressed genes, compared to the genomic average. Melting energies were computed with the parameters of Santa Lucia (49) and averaged over each window.

RESULTS

In *Salmonella enterica*, the single *ihfA* and *ihfB* mutants and the double *ihfA*/*ihfB* mutant show similar growth characteristics (29). In contrast, in *D. dadantii* 3937 the *ihfB* mutation severely compromises growth (36) but not the *ihfA* mutation; we therefore took advantage of the latter to disable the formation of the IHF heterodimer in *D. dadantii* cells. In *E. coli*, it was observed that, potentially, both IHFα and IHFβ could form homodimers capable of binding DNA

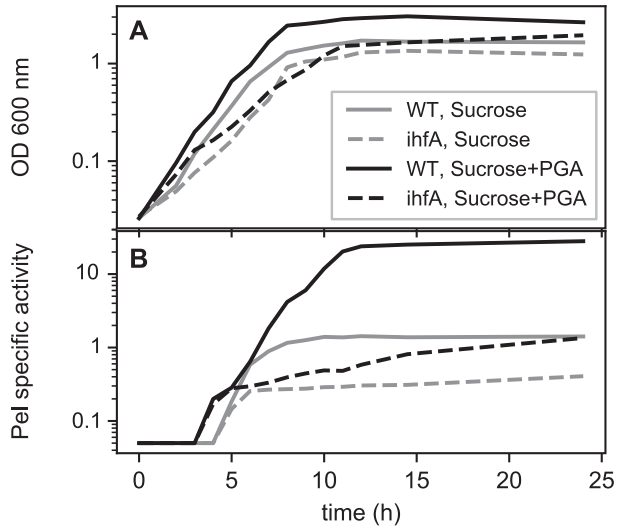

Figure 1. (**A**) Growth and (**B**) pectate lyase production of *Dickeya dadantii* 3937 wild type strain (solid lines) and its *ihfA* derivative (dashed lines) grown in liquid M63 minimal medium supplemented with sucrose (gray) or sucrose+polygalacturonate (black). Samples were taken every hour. Pel specific activity is expressed as μmol of unsaturated product liberated per min per mg of bacterial dry weight. The experiment was repeated three times and curves from a representative experiment are shown (variation between experiments was less than 15%).

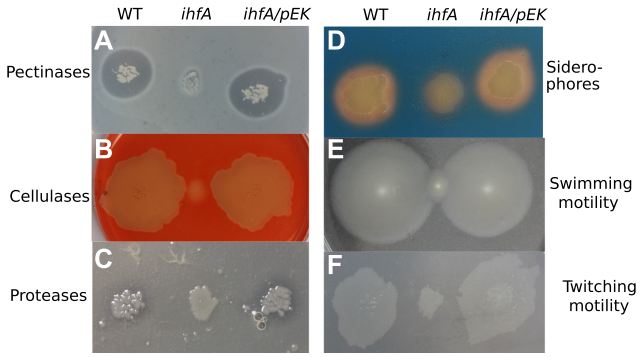

Figure 2. Phenotypes of the *D. dadantii ihfA* mutant and its complemented derivative *ihfA*/pEK. (**A**) Pectinase activity was observed after growth on PGA-containing plate and staining with copper (II) acetate solution. (**B**) Cellulase activity was detected after growth on Carboxy-Methyl Cellulose-containing plate, followed by staining with Congo red. (**C**) Protease activity was revealed, after growth on skim milk-containing plate by a translucid halo surrounding the bacteria growth area. (**D**) Siderophore production was detected after growth on chrome azurol S (CAS) agar plate. (**E**) Swimming motility inside the soft agar medium, was estimated by picking bacterial colonies with a thin rod inside a semi-solid agar plate containing low concentration of agar (0.4% w/v). (**F**) Twitching motility at the surface of the agar medium was estimated by picking bacterial colonies with a thin rod inside a standard agar plates containing carboxy-methyl cellulose (0.2% w/v) and glucose (0.2% w/v). Plates were incubated at 30°C for 24 h before measuring colony expansion.

and supporting the lambda phage site-specific recombination reaction *in vitro* (50). However, the binding affinity of the IHFβ homodimer is by two orders of magnitude lower than that of the IHF heterodimer, whereas IHFα homodimer is highly unstable (51,52). In *D. dadantii*, we observed that the *ihfA* mutant is able to grow and achieve, albeit with delay, reasonably high cell densities (Figure 1A), making it amenable to experimental investigation. Given the fact that the lack of IHF is more detrimental for *D. dadantii* than for *E. coli* (36) and that the *ihfB* gene expression is unaffected in *ihfA* mutant (Supplementary Table S2 in Supplementary Materials), as also observed in *E. coli* (33), it is conceivable that bacterial growth is supported by the activity of the low-affinity IHFβ homodimer. In this study, we assume that all alterations induced by *ihfA* mutation reflect the *deficiency* of the active IHF heterodimer in the cell, with the caveat that the low affinity IHFβ homodimer may provide a 'buffering' effect alleviating the detrimental effect of the complete absence of IHF.

IHF regulates cell motility, production of plant cell wall degrading enzymes, siderophores and cell aggregation

Inactivation of *ihfA* resulted in reduced production of many virulence factors such as pectinases (mainly pectate lyases), cellulases and proteases responsible for the destruction of the plant cell wall and production of the soft rot symptoms (Figure 2A–C). The *ihfA* mutation also reduced the production of siderophores (Figure 2D) required for the systemic progression of maceration symptoms in the hosts (53,54). Furthermore, the swimming and twitching capacities of *D. dadantii* essential for searching favourable sites of entry into the plant apoplast were reduced (Figure 2E and F). Complementation of the *ihfA* mutant with the *ihfA* gene carried on the pEK plasmid restored the WT phenotype in all cases, indicating that inactivation of *ihfA* was responsible for impaired functions (Figure 2).

D. dadantii produce cellulose fibrils, which enable the cells to aggregate on the plant surface and form a biofilm resistant to desiccation (37). The cellulose fibrils are not required anymore when bacteria enter into the plant apoplast and colonize this inter-cellular compartment by using their motility function. Cell aggregate formation was analysed in the WT and *ihfA* strains grown under low shaking conditions (Figure 3). We found that the growth medium of both the WT strain and the complemented *ihfA* mutant appeared turbid and at the bottom of the tubes, only small cell aggregates were observed (Figure 3A). In contrast, the growth medium of the *ihfA* mutant was clear and a large cell aggregate was observed (Figure 3A). The estimated percentages of cells in aggregates were 29% for the WT strain, 37% for the complemented *ihfA* strain and 76% for the *ihfA* mutant (Figure 3B). Inactivation of the *bcsA* gene encoding cellulose synthetase suppressed the aggregation phenotype observed in the *ihfA* mutant. Taken together, these results demonstrate that IHF deficiency up-regulates the production of cellulose fibril adherence structures.

Inactivation of *ihfA* strongly reduces pectinase activity and impairs *D. dadantii* virulence

Since the soft rot symptoms of infection by *D. dadantii* are mainly due to the production and secretion of pectate lyases (Pels), we monitored the production of Pels and their induction by polygalacturonic acid (PGA, a pectin derivative) in both *ihfA* and WT cells.

As mentioned above, compared to the WT strain, the *ihfA* mutant exhibited a slower growth rate, reaching lower max-

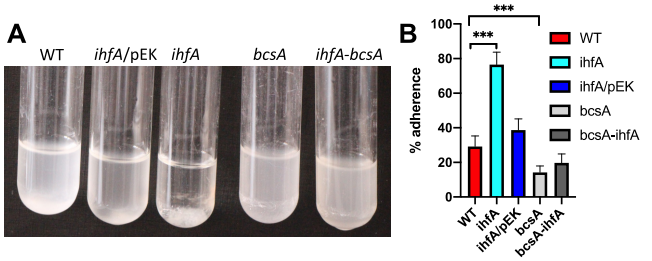

Figure 3. (**A**) Aggregation phenotype of the *D. dadantii* 3937 WT strain and its derivatives, *ihfA*, *bcsA*, *ihfA-bcsA* and the complemented *ihfA*/pEK strain. Strains were grown in minimal M63 medium supplemented with glycerol for 48 h under low shaking condition (55 rpm). (**B**) Quantification of the cells present in the aggregates and in the planktonic fractions for the different strains; each value represents the mean of five experiments and bars indicate the standard deviation. *** indicates a significant difference relative to the WT ($P < 0.001$, Mann–Whitney test).

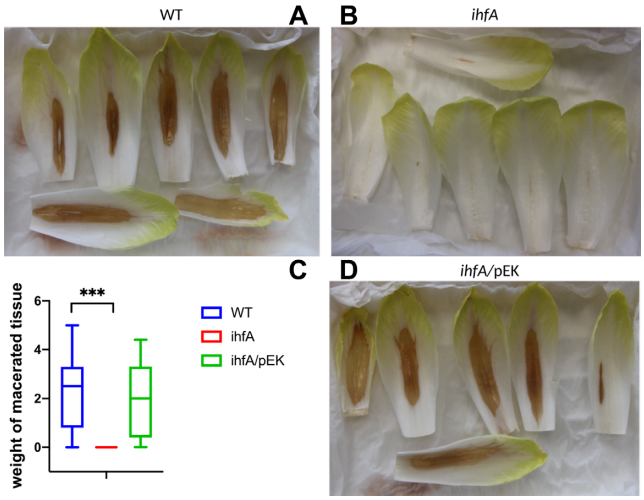

Figure 4. Maceration capacity of WT, *ihfA* and *ihfA* complemented (*ihfA*/pEK) strains on chicory leaves. Representative specimen of chicory leaves infected by the wild-type strain (**A**), the *ihfA* mutant (**B**), the complemented *ihfA*/pEK strain (**C**). One hundred chicory leaves were infected for each strain, using 5 µl of bacterial suspension (10^8 cfu ml^{-1} in 50 mM KH_2PO_4 pH 7 buffer). After incubation in a humid chamber for 24 h at 30°C, the weight of macerated tissue was measured. (**D**) Boxplot from 100 data points. The calculated median value is 2.5 g of macerated tissue for the WT strain, 0 g for the *ihfA* mutant and 1.9 g for the complemented *ihfA*/pEK strain. Centre lines show the medians; box limits indicate the 25th and 75th percentiles. *** indicates a significant difference relative to the WT ($P < 0.001$, Mann–Whitney test).

imal densities both in presence and absence of PGA (Figure 1A). In the *ihfA* mutant, the production of Pels was strongly reduced at all sampling times both in PGA-induced and non-induced growth condition, while the growth phase-dependence of Pel production was retained (Figure 1B). However, the most striking effect was the strongly reduced induction by PGA, as the production of Pels was weaker in the *ihfA* mutant in presence of PGA than in the WT strain in absence of inducer (but it kept increasing slowly due to the low remaining Pel enzymatic activity).

Altogether, these observations suggest that IHF plays a central role in *D. dadantii* pathogenicity by activating several key virulence factors. We therefore analysed the impact of *ihfA* mutation on *D. dadantii* virulence, using the chicory leaf assay (Figure 4). As expected, the pathogenic growth is drastically reduced when the plant is infected with the mutant strain. Complementation of the *ihfA* mutation with the *ihfA* gene carried on the pEK plasmid fully restored the virulence. This result indicates that IHF heterodimer is required for the development of soft rot disease induced by *D. dadantii* in chicory.

The *ihfA* mutation reorganizes the *D. dadantii* transcriptome

As seen above, the strong phenotypic effect of the *ihfA* mutation results from the inactivation of several key virulence functions. To broaden this observation and assess the role of IHF in global gene regulation, we analysed the *D. dadantii* transcriptome by RNA-seq under various growth conditions: in early exponential phase in M63 minimal medium supplemented with sucrose as carbon source, and at transition to stationary phase in M63 supplemented with either sucrose or sucrose + PGA (see Materials and Methods).

The most dramatic effect of IHF on gene regulation was observed when the transcriptomes were compared in presence vs absence of PGA, in both *ihfA* and wild type cells. Whereas 762 and 752 genes were found respectively up- and down-regulated by PGA in the wild-type strain, only about a dozen of genes were altered in the *ihfA* background under the same conditions (Supplementary Table S1). This finding is fully consistent with the impaired cell wall-degrading enzyme activity in *ihfA* strain described above (Figures 1B and 2) and indicates that the mutant almost completely lost the ability to metabolise this important energy source in the medium.

In order to analyse the regulatory effect of IHF, we next focused on the transcriptomes obtained with sucrose as sole carbon source (Supplementary Table S2). We found that 809 genes in total were differentially expressed during the exponential and stationary phases in the WT vs *ihfA* transcriptome comparisons (Figure 5A). This large number exceeds that of the differentially expressed genes reported in *E. coli* using DNA microarray analysis (28), and is consistent with the notion that IHF acts as a global regulator in *D. dadantii* 3937. Among these genes, 432 were differentially expressed during exponential growth and 682 during stationary phase, consistent with the major impact of IHF at this stage of growth (26). Out of the 809 differentially expressed genes, 365 fell into the category of 'IHF-repressed' (*i.e.* up-regulated in *ihfA* mutant) and 444 fell into the category of 'IHF-activated' (i.e. down-regulated in *ihfA* mutant). These 809 differentially expressed genes reflect both direct and indirect regulation by IHF.

Functional classes of differentially expressed genes

An analysis of the biological functions significantly enriched among differentially expressed genes in the *ihfA* mutant (Figure 5) suggests a global reorganization of the central metabolism, including carbon storage via gluconeogenesis, use of alternative carbohydrate (galacturonate, arabinose, mannose) catabolic pathways and reduction in the biosynthesis of fatty acids and nucleotides. Such observations are indicative of a profound modification in carbon

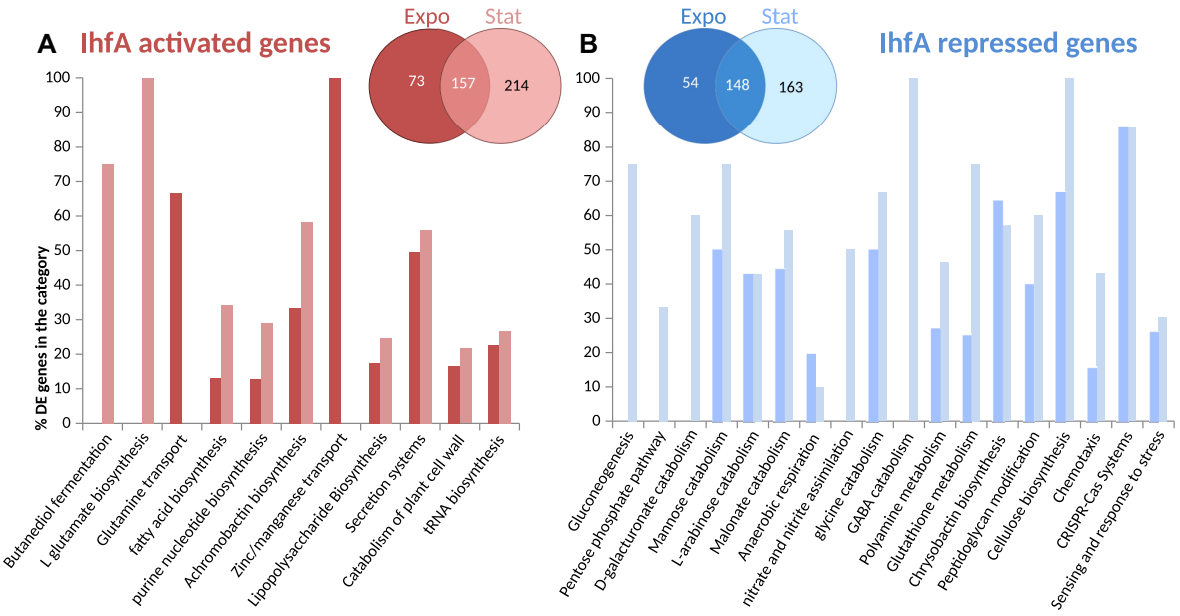

Figure 5. Transcriptional response to *ihfA* mutation. Venn diagram and functional repartition of genes significantly activated (**A**) or repressed (**B**) in the *ihfA* vs WT strain. Only genes with an adjusted *P*-value < 0.05 and fold-change > 2 (either positive or negative) were considered.

flow. A preference towards anaerobic metabolism was observed, with an increase in malonate catabolism, increase in the pentose phosphate pathway in connection with the capacity to regenerate the redox potential (NADPH) of cells. Nitrogen metabolism was also affected with an increased assimilation of nitrate and nitrite as well as an increase in the catabolism of amino acids (Glycine and GABA catabolism) and polyamines. This profile is consistent with the role of IHF in regulation of RpoN-dependent genes (18,55) and nitrogen regulation, as also observed in *Klebsiella pneumoniae* (56) and *Rhizobium meliloti* (57).

In *ihfA* mutant cells, numerous virulence functions were down-regulated, including the secretion systems Prt T1SS, Out T2SS, Hrp T3SS, T6SS as well as their effectors. Genes encoding plant cell wall-degrading enzymes including proteases PrtABCG secreted by T1SS, pectinases Pels, cellulase Cel5Z, xylanase XynA secreted by T2SS were down-regulated as well as other type 2 effectors such as the extracellular necrosis inducing protein NipE and the two proteins AvrL-AvrM favouring disease progression. Genes encoding the type 3 effectors (DspE, HrpN, HrpW) which suppress plant immunity and promote pathogenesis were down-regulated as well as the genes encoding type 6 effectors (RhsA, RhsB) which have been identified as antibacterial effectors but may have key functions within the plant host (58). Furthermore, the *rhlA* gene responsible for biosurfactant biosynthesis promoting plant surface colonization was down-regulated (6). Biosynthesis of the two siderophores, which allow bacteria to cope with the restricted iron bioavailability in the plant (53,59,60) and which also manipulate plant immunity (54) was distinctly affected in *ihfA* mutant: achromobactin, which is produced when iron becomes limiting was down-regulated, whereas chrysobactin prevailing under severe iron deficiency was up-regulated. In addition, *ibpS* and *indABC* genes responsible for production of an iron scavenging protein (61) and of the antioxidant pigment indigoidine (62) respectively, were down-regulated. Regarding motility, the *pil* genes involved in twitching motility were down-regulated, but the flagellar genes were not significantly affected. Also the genes encoding several important regulators of virulence were affected: the repressor gene *pecT* was up-regulated while the nucleoid-associated protein gene *fis* was down-regulated, as well as the genes of regulators *hrpL, mfbR, fliZ* and the small non-coding RNA *rsmB* (Supplementary Table S2).

Overall, the decrease in anabolic functions concomitant with an increase in catabolic functions provides a signature of the 'survival mode' behavior of the *ihfA* mutant, consistent with modifications of the bacterial envelope (peptidoglycan, outer-membrane porins, lipopolysaccharide, exopolysaccharide in particular cellulose), and with an increased stress response and activation of the CRISPR-Cas defences.

We shall note however, that the number of genes among these enriched functional groups represented only a half of the total number of differentially expressed genes. The other half was more dispersed among various pathways, making it difficult to allocate them to particular functions.

IHF binding predictions at gene promoters

We next attempted to get an insight into the mechanism underlying the regulatory effect of IHF. The latter is known to act as a global transcription factor binding at many gene promoters but, in contrast to the closely related NAP HU, IHF recognizes a relatively well-defined sequence motif (WWW**TCA**ANNNN**TTR**) (63), possibly related to the extreme bend of about 180° that it introduces in the DNA (15). We took advantage of this feature to predict the distribution of potential IHF binding sites in the chromosome, and assess which responsive genes are possibly regulated through a direct activation or repression of their promoter

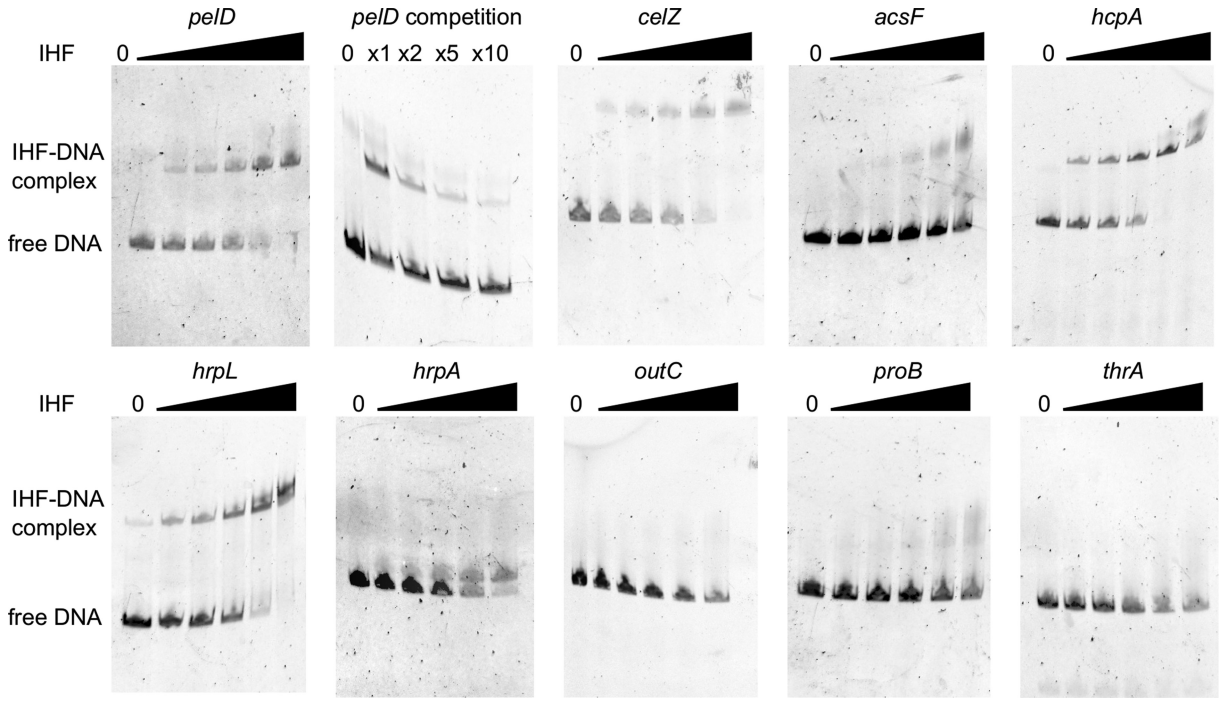

Figure 6. Interaction of IHF with the regulatory regions of various genes. For each band shift assay, 100 ng of FAME-labeled DNA were incubated with 0, 10, 15, 25, 50, 100 nM IHF. *pelD* competition was performed in presence of 25 nM IHF with 2X, 5X, 10X unlabeled *pelD* DNA. The experiments were performed three times and a typical result is shown.

by IHF. The results are provided in Supplementary Table S5 in Supplementary data, with predictions filtered with a loose threshold (5500 putative binding sites retained, this list is used in the following paragraphs). Around 36% of the 809 differentially expressed genes have an upstream IHF binding signal, with a weak but significant enrichment compared to the proportion obtained with random sets of genes of identical size (31% in average, P-value = 0.007). Keeping only 500 sites with strongest scores reduced this proportion to 8%, but the relative enrichment became stronger (5% for random genes, P-value = 0.003).

The relevance of these *in silico* predicted IHF binding sites was tested on different classes of promoters via band shift experiments. The purified IHFαβ was found to bind the promoter regions of several genes regulated by IHF in the transcriptomes and containing DNA sequences with good matches to the IHF motif: *pelD* (pectate lyase D), *cel5Z* (cellulase), *acsF* (achromobactin siderophore), *hrpL* and *hrpA* (type 3 secretion system), *hcpA* (type 6 secretion system) (Figure 6). Therefore, all these genes are most likely directly regulated by IHF. By contrast, no shifted complex was observed for the *outC* gene (type II secretion system) that exhibits an altered expression in the *ihfA* mutant but does not contain IHF binding site, consistent with an indirect regulation of *outC* by IHF. No shifted complexes were detected with the two negative controls *thrA* and *proB* not differentially expressed in the *ihfA* mutant and exhibiting no predicted binding site. Based on this limited set of promoters, the *in silico* IHF binding site predictions are in good agreement with the presence of an *in vitro* IHF-DNA interaction detected by band-shift assays (Figure 6), as we expected from the relatively well-defined sequence motif of IHF. This observation supports the proportions of directly vs indirectly regulated promoters computed above. On the other hand, there is only a limited quantitative correlation between the computed scores and the observed binding affinities, showing that the predicted interaction strengths cannot not be reliably compared among promoters bound by IHF, as also expected from the intrinsic limitations of sequence motifs which do not take into account the environment of the promoter, presence of mechanical deformations, other proteins, etc.

The computations above suggest that only a limited fraction of the IHF regulon is involved in a direct interaction with the protein. This behaviour deviates from that of many specific transcriptional regulators targeting a small number of promoters, but is expected for a 'hub' of the regulatory network such as IHF, which activates or represses many genes in an indirect manner.

Additionally, IHF is known to act not only as a 'digital' transcription factor, as we have considered so far, but also as a NAP that binds DNA with loose specificity, and modulates the transcriptional activity by an 'analogue' mechanism (64) involving global modifications of the chromosome architecture. It is the latter mechanism that we now investigate in more detail.

Regulatory interplay between IHF and DNA supercoiling

One of the major factors in bacterial chromosome compaction and analogue transcriptional regulation is DNA supercoiling, which is controlled by a crosstalk between the topoisomerase enzymes and the NAPs (10). We therefore addressed the question of possible coupling between the

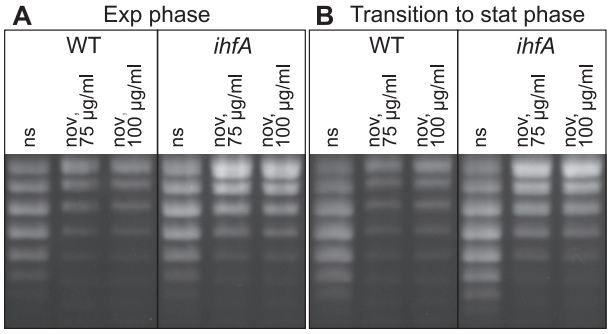

Figure 7. DNA supercoiling in the *D. dadantii* WT strain and its *ihfA* derivative. Topoisomers of plasmid pUC18 were isolated and separated on agarose gel containing 2.5 µg ml^{-1} chloroquine. At this concentration, the more negatively supercoiled topoisomers migrate faster in the gel. The experiment was performed three times and a typical result is shown. Growth phases and novobiocin treatment are indicated (ns, none stressed cells).

regulatory action of IHF and changes of DNA topology. Such an effect was shown to underpin the IHF regulation of the *ilvP* promoter of *E. coli* (65), but was never investigated at the genomic scale in an enterobacterium.

We monitored the effect of IHF on global DNA topology by high-resolution agarose gel-electrophoresis of pUC18 plasmids isolated at different stages of growth from both WT and *ihfA* mutant strains grown with or without treatment by the gyrase inhibitor novobiocin (Figure 7). Whereas addition of novobiocin induced a comparable relaxation of DNA in both strains (of $\Delta\sigma > 0.006$) the *ihfA* mutant did not exhibit any significant change in DNA topology compared to the WT strain. This observation is consistent with the lack of variation in topoisomerase gene expression in the *ihfA* transcriptome (Supplementary Table S2) and can be related to previously observed similar contrasting effects of *fis* and *hns* mutations in *D. dadantii* and *E. coli* (14,25).

Given that *ihfA* mutation has no noticeable impact on global topology of plasmid DNA, is it equally irrelevant with regard to the supercoiling response of chromosomal genes? To answer this question, we monitored the transcriptional response of the WT and mutant strains to novobiocin treatment (Supplementary Table S3). The number of genes significantly activated or repressed in response to novobiocin addition was slightly lower in *ihfA* mutant (774 in exponential phase, 809 on transition to stationary phase) than in the WT strain (914 and 1133 genes, respectively). Strikingly, however, the genes sensitive to gyrase inhibition in the two strains were mostly different (Figure 8A). Furthermore, the effect of the *ihfA* mutation differed depending on the supercoiling level of the DNA, with many genes responding specifically in the relaxed state of the chromosome (Supplementary Table S4 in Supplementary Data). A set of functional pathways belonging to sugar catabolism (ribose, lactose), amino-acid biosynthesis (leucine, valine, isoleucine, tryptophan, histidine), malate and ureide catabolism, flagellar assembly and disulfide bond formation was enriched in this group. Among the plant cell wall-degrading functions, the galactan catabolism was specifically repressed (Figure 8B).

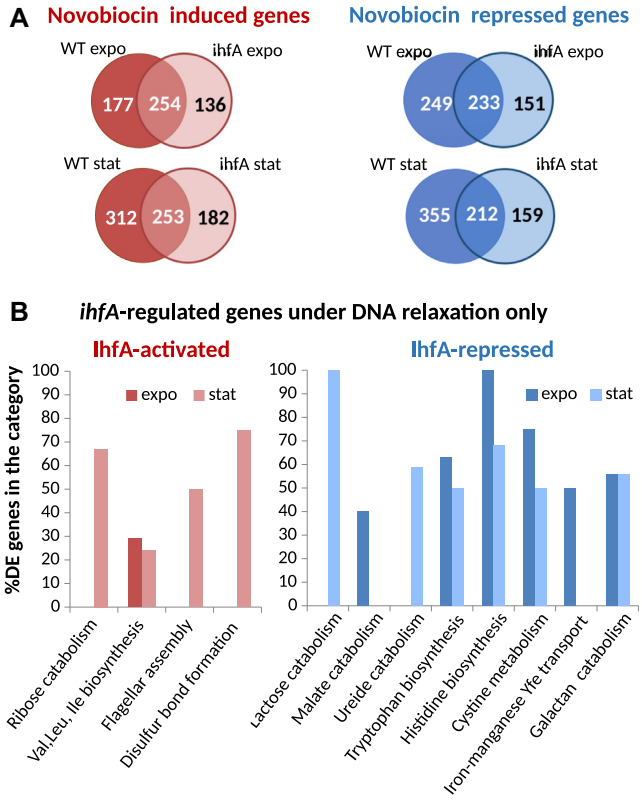

Figure 8. Transcriptional response to global DNA relaxation induced by novobiocin treatment of the *D. dadantii* WT and *ihfA* strains. (**A**) Venn diagrams of significantly activated and repressed genes after a novobiocin shock, either in the WT or *ihfA* strains, in exponential and stationary phases. Only the significant differentially expressed genes (P-value < 0.05, Fold-Change > 2 or Fold-Change < 0.5) were considered. (**B**) Functional gene groups significantly enriched among the *ihfA*-regulated genes under conditions of DNA relaxation. A statistical enrichment analysis was carried to extract biological processes significantly over-represented in the set of *ihfA*-regulated genes under conditions of DNA relaxation.

This nontrivial response to DNA relaxation by novobiocin indicates that, although the *ihfA* mutation apparently does not change the *global* supercoiling level of DNA, it has a strong impact on how gyrase affects transcription at the genomic scale, which, in turn, likely reflects a profound modification of the *local* distribution of DNA supercoiling along the chromosome. We now analyse this phenomenon at two successive length-scales.

Orientational organisation of IHF transcriptional regulation by genomic architecture

Gyrase inhibition is known to affect the gene expression globally, but with a bias for convergent genes, i.e. genes located on complementary DNA strands and facing each other (47). This effect is related to the asymmetric build-up of positive and negative supercoils during the transcription process itself, which underpins an intimate regulatory coupling between transcription and DNA supercoiling and affects neighbouring genes differently depending on their relative orientation (47). Interestingly, whereas DNA relaxation by novobiocin in WT cells reduces the transcription

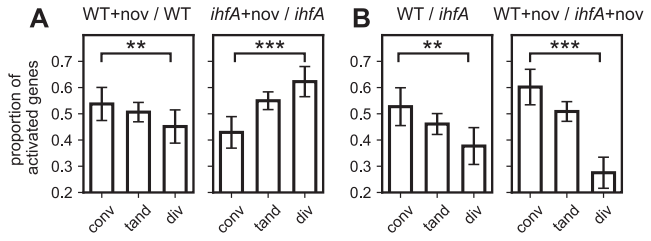

Figure 9. Local organisation of IHF transcriptional regulation by genomic architecture. (**A**) Proportion of activated genes among differentially expressed (activated+repressed) convergent, tandem and divergent genes during gyrase inhibition by novobiocin, in the WT strain and its *ihfA* derivative. The selective activation of convergent vs divergent genes is completely reversed in the absence of IHF. (**B**) Comparison of the transcriptional effect of *ihfA* mutation to WT depending on gene orientation, in absence and presence of novobiocin. All proportions are computed at the transition to stationary phase. Error bars represent 95% confidence intervals.

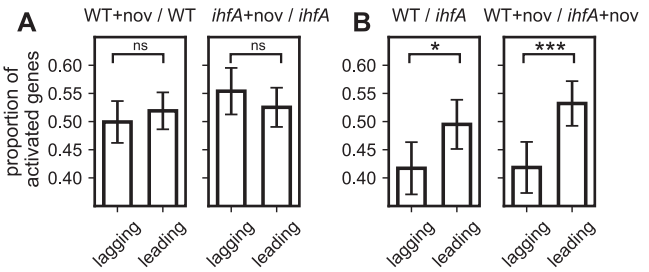

Figure 10. Effect of IHF on the leading versus lagging strand utilisation. (**A**) Proportion of activated genes among the differentially expressed genes on the leading and lagging strand during gyrase inhibition by novobiocin, in the WT strain and its *ihfA* derivative. Note the selective activation of lagging strand transcription in the absence of IHF. (**B**) Comparison of the transcriptional effect of *ihfA* mutation to WT on the genes expressed on the leading and lagging strand in absence and presence of novobiocin. All proportions are computed at the transition to stationary phase. Error bars represent 95% confidence intervals.

of divergent genes (Figure 9A, left panel), the lack of IHF heterodimer in the *ihfA* mutant completely reverses this effect, with divergent genes being more activated than convergent ones (Figure 9A, right panel). This means that IHF heterodimer plays a crucial role in organising the DNA supercoils in the vicinity of transcribed genes, consistent with the proposed effect of IHF on gyrase binding at 3′-ends of transcription units (24). The relation between gene orientation and IHF regulation can be also analysed by comparing the gene expression of the two strains (Figure 9B). Whereas the presence of IHF heterodimer already favours convergent genes in standard growth conditions, the effect is considerably enhanced in a novobiocin-relaxed chromosome, with more than a 2-fold higher proportion compared to divergent genes. This effect likely results from the combination of two factors: (1) divergent regions are more AT-rich, and would thus tend to attract IHF heterodimer more favourably than convergent ones, due to AT-rich IHF binding site consensus (63), as visible in the distribution of predicted binding sites (keeping in mind their limitations, as stated above, Supplementary Figure S1 in Supplementary Materials); (2) IHF is known to recognise the structural properties (geometry) of DNA as well as its sequence (66) and its binding might thus also be modulated differently by DNA supercoils resulting from adjacent transcription in these regions. This differential effect of IHF on the convergent and divergent transcription units raised the question about its possible influence on the directionality of genomic transcription.

We therefore analysed the preferences of leading and lagging strand transcription in the WT and *ihfA* mutant cells. We found that DNA relaxation by novobiocin addition has no effect on leading versus lagging strand utilization, whether in the WT or in the *ihfA* mutant cells (Figure 10A), suggesting that gyrase activity does not impose any preferences for strand utilization. On the other hand, when we compared the expression of genes between the WT and *ihfA* mutant cells, we found that on average, the leading strand utilization was significantly preferred in the WT cells, consistent with the proposed recruitment of gyrase by IHF at the ends of transcription units and facilitated relaxation of positive superhelicity accommodated in front of the translocating RNA polymerase (24). Interestingly, high levels of superhelical density characteristic of exponential growth favor leading strand utilization (67), while the effect of IHF was enhanced under conditions of DNA relaxation (Figure 10B) consistent with the notion that IHF preferentially binds relaxed DNA (68) and the role of IHF in nucleoid packaging in stationary phase (22). Thus, depending on the supercoiling regimen, IHF heterodimer determines the extent of preference of leading and lagging strand utilization imposing directionality on genomic transcription.

Taken together, these results suggested that *ihfA* mutation may cause a global reorganization of genomic transcription especially in response to changes of DNA supercoiling and in particular, affect the organization of CODOs.

Global organisation of IHF transcriptional regulation in chromosomal regions

In order to describe how IHF regulation is distributed along the chromosome we enlarged the scanning window of our analysis (Figure 11). At the megabase scale, the genome of *D. dadantii* exhibits a symmetrical organisation into four large regions (11) of various G/C contents or DNA thermodynamic stabilities (denoted SD1, SD2, LD1, LD2, outer wheel of Figure 11A), which are highly conserved among *Dickeya* species (13). The predicted binding of IHF (second outer wheel) follows the same pattern, which likely reflects the protein's preference for AT-rich sequences (63), but may also entail a relation between DNA physical properties and the binding and regulation by IHF. Such a relation was previously observed for the two NAPs FIS and H-NS, leading to the identification of eleven coherent 'stress-response' domains (aka CODOs) exhibiting distinct DNA physical properties and responses to NAPs, growth conditions and environmental stresses (11,13).

The four inner rings in Figure 11, show the genomic distributions of up-regulated (red; z-score >2 indicating a statistically significant enrichment in the considered 500 kb region) and down-regulated (blue; z-score < -2) genes, either between WT and *ihfA* in various conditions (inter-strain comparison, A), or between cells with and without novobiocin treatment (intra-strain comparison, B). The inter-

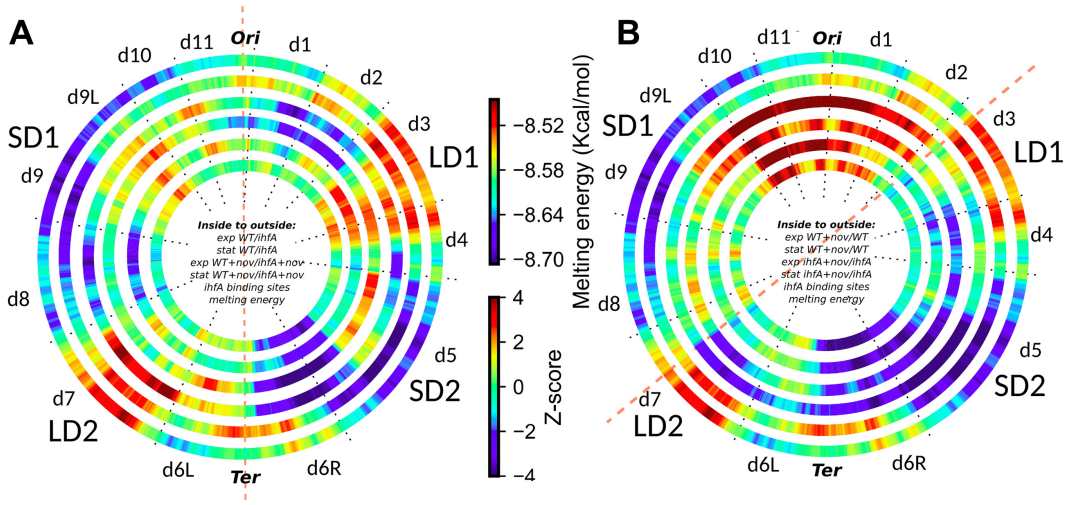

Figure 11. Chromosomal wheels showing the global organisation of IHF transcriptional regulation in *D. dadantii* genome. (**A**) Two inner rings: inter-strain comparison (WT vs *ihfA*) in exponential (innermost ring) and stationary (second ring) growth phases; two middle rings, the same but under conditions of DNA relaxation by novobiocin. Red and blue colors respectively indicate a significantly enriched density of activated and repressed genes in a 500 kb window, compared to the genomic average. Outermost ring: distribution of DNA thermodynamic stability of the *D. dadantii* 3937 genome. Second outer ring: local enrichment in predicted IHF binding sites. (**B**) Two inner rings: intra-strain (WT vs Wt+novo) comparisons in exponential (innermost ring) and stationary (second ring) phase. Two middle rings, the same as inner rings, but for *ihfA* vs *ihfA*+novo comparison. Densities of novobiocin-induced (red) or -repressed (blue) genes in wild-type or *ihfA* mutant cells are indicated as in A. Two outer rings: same as in A. The red dashed line in A indicates the OriC-Ter axis. The red dashed line in B separates the two, apparently more activated and more repressed halves of the chromosome in response to DNA relaxation.

strain comparison clearly shows that the regulatory impact of IHF is organised into extended regions displaying coherently activated or repressed genes largely corresponding to the previously identified CODOs. Among these, some regions are regulated by IHF independent of the growth phase and DNA supercoiling (e.g. activation of d9L and d3, as well as repression of d6R). Some appear regulated by IHF independent of DNA supercoiling but in a growth phase-dependent manner (e.g. d8), while some others (e.g. d2) are specifically repressed under conditions of DNA relaxation, independent of the growth phase. Finally, some regions are specifically activated under conditions of DNA relaxation but only at a particular stage of growth (d5 in exponential phase and d7 in stationary phase).

The intra-strain profile of wild type cells was fully consistent with the previously observed pattern (11) and demonstrated that independent of the growth phase, the relaxation of DNA regulates the transcriptome in a remarkably polar way, activating the chromosomal OriC end and repressing the Ter end (Figure 11B, two innermost rings). Independent of the growth phase, both the activation and repression by DNA relaxation extended much further away from the Ori/Ter axis in *ihfA* mutant compared to WT, abutting in the right and left arms at the two AT-rich regions LD1 and LD2 respectively and thus, suggesting that in absence of IHF heterodimer the supercoiling response is strongly correlated to the thermodynamic properties of the genomic sequence.

The comparative analysis of the inter- and intra-strain transcript patterns reveals the combinatorial effects of NAPs and DNA supercoiling (25). Overall, we observed a conspicuous asymmetry in the IHF-dependent transcription pattern of the left and the right chromosomal arms, which is especially enhanced under conditions of DNA relaxation. For example, independent of the growth phase, the Ter region is split into two, left (d6L) and right (d6R) halves showing different expression levels (on both sides of OriC-Ter axis indicated by red dashed line in Figure 11A). Note also the difference between the activities of the CODO's d11 and d1 on both sides of the Ori end, again especially conspicuous under conditions of DNA relaxation. Thus, on DNA relaxation the IHF-dependent expression pattern of replichores along the OriC-Ter axis of the chromosome becomes more asymmetric. In contrast, the bidirectional extension of activation and repression of the genomic transcription from respectively the OriC and Ter ends induced by DNA relaxation (intra-strain pattern, Figure 11B), makes the genomic expression pattern more uniform in the *ihfA* mutant compared to WT cells. The genome appears divided into two, predominantly activated and predominantly repressed halves, apparently delimited by the thermodynamically labile LD1 and LD2 regions presumably enriched for putative IHF binding sites (dashed red line in Figure 11B). These observations point to an implication of the IHF heterodimer, either directly or indirectly, in the establishment of boundaries precluding the spatial expansion of the transcriptional response to DNA supercoiling.

DISCUSSION

The aim of this study was to determine the effect of the nucleoid-associated protein IHF on pathogenic growth and global gene expression in the model of *D. dadantii*. Since IHF is a component of an overarching network comprising DNA topoisomerases and highly abundant NAPs, serving both as chromatin shaping factors and global regulators of genomic transcription (69), the effects on gene expression reported here are mediated in part by direct impact of IHF

binding at gene promoters, but also by changes in the network components induced by the lack of the functional IHF heterodimer in the cell. Our previous studies demonstrated that inactivation of two other representatives of this class of global regulators, FIS and H-NS, strongly attenuate the pathogenic potential of *D. dadantii* (4,14,70). In this work we show that mutation of *ihfA* precluding the formation of IHF heterodimer in the cells dramatically alters the transcript profile, retards cellular growth, modulates the transcriptional response to DNA relaxation by novobiocin, impairs the expression of virulence genes and as a result, abrogates the virulence of *D. dadantii* 3937. Thus, it appears that all these NAPs acting both as sensors of environmental conditions and global transcriptional regulators (69) are directly involved in coordinating the *D. dadantii* pathogenicity function with environmental conditions. The dramatic effect of *ihfA* mutation on pathogenic potential results primarily from the inability of *ihfA* mutant to utilize pectin, an important carbon source provided by the plant host, due to impaired production and/or secretion of the plant cell wall degrading enzymes, especially the Pels. This inability is reflected in the huge difference in the amount of differentially expressed genes between the WT and *ihfA* mutant strains grown in the presence of PGA, which is degraded by wild-type cells but not by the mutant (Supplementary Table S1).

Correspondence between phenotypes and relevant genes

The phenotypic traits affected by *ihfA* mutation in *D. dadantii* are by large similar to those reported in a recent study of *Dickeya zeae* strain lacking IHF (34). However, with the possible caveat that the IHFβ homodimer might alleviate the effect of the lack of IHF heterodimer in *ihfA* mutant of *D. dadantii*, there are also interesting differences. For example, the *D. zeae* cells lacking IHF demonstrate decreased motility and biofilm forming capacity. In *D. dadantii* the motility is also impaired (Figure 2), but the formation of adherence structures is increased (Figure 3). This latter phenotype is consistent with increased expression of genes involved in production of cellulose and exopolysaccharide (Supplementary Table S2). Motility and chemotaxis are essential for *D. dadantii* when searching for favourable sites to enter into the plant apoplast, as mutants with affected flagella or chemotaxis transduction system are avirulent (71). Flagellar and chemotaxis genes are significantly affected in the *ihfA* mutant under conditions of DNA relaxation (Supplementary Table S4). This includes the *fliZ (CODO 7)* gene (Supplementary Table S2) encoding the regulator of flagellar genes involved in decision between the alternative lifestyles, namely, between flagellum-based motility and biofilm formation (72) and might explain the altered motility and formation of adherence structures observed in *D. dadantii ihfA* mutant (Figures 2 and 3). The *pil* genes encoding the type IV pilus are down-regulated, in keeping with the impaired twitching motility of the *ihfA* mutant (Supplementary Table S2 and Figure 2). The importance of type IV pilus responsible for twitching motility in *Dickeya* pathogenicity has not been studied yet. However, type IV piliation was shown to contribute to virulence in other plant pathogens, mainly in vascular pathogens, such as *Ralstonia* and *Xylella*, where they were proposed to contribute to bacterial colonization and spread in the xylem through cell attachment and twitching motility (73).

In general, the observed phenotypic changes are closely reflected in the *D. dadantii* transcriptome. The global decrease in pectinase, cellulase and protease production in the *ihfA* mutant (Figure 2) is consistent with the impaired expression of both their cognate secretion systems (T1SS PrtEFD for proteases and T2SS OutCDEFGHIJKLMNO for pectinases and cellulase) and their coding genes (*pelA, pelC, pelZ, pelI, pelN, celZ, prtA, prtB, prtC, prtG*) (Supplementary Table S2). It is noteworthy that expression of several *pel* genes (*pelB, pelD, pelE*, *pelW, pelX)* is not significantly affected in non-inducing conditions (Supplementary Table S2) but expression of these genes is strongly decreased in the presence of inducer PGA (Supplementary Table S1). The *pel* genes are regulated by a large number of global and dedicated transcription factors including H-NS, FIS, CRP, PecT, PecS, KdgR, MfbR and by the RsmA/RsmB post-transcriptional regulatory system (2). This requirement of complex regulation likely reflects the adaptation of the bacterial lifestyle to adverse conditions of growth in various hosts, demanding a fast and reliable production of virulence factors. Expression of several regulatory genes including *fis, pecT, mfbR*, as well as the *rsmB* gene encoding regulatory sRNA, is controlled by IHF (Supplementary Table S2). The dedicated transcriptional repressor PecT *(CODO 7)* is repressed by IHF, and its overproduction might contribute to the plant cell wall-degrading enzyme defective phenotype of *ihfA* mutant. Indeed, a similar phenotype linked to PecT de-repression was observed in *hns* mutant (74). The decreased expression of *fis* and *mfbR* in the *ihfA* background (Supplementary Table S2) might also affect the nucleoprotein complex formed at the *pel* promoters so that it is incapable to sustain *pel* expression (75). Indeed, MfbR is known to activate genes encoding plant cell wall-degrading enzymes in response to alkalinisation of the apoplast during the advanced stage of infection (76). Similarly, the down-regulation of *rsmB* gene observed in *ihfA* mutant can also explain the decreased plant cell wall-degrading enzyme production (Supplementary Table S2). Indeed, RsmB is a small RNA involved in the post-transcriptional control of the RNA-binding protein RsmA, which turns down the production of pectate lyases by binding directly to the *pel* mRNAs (77). RsmB carries multiple RsmA binding sites and, therefore, titrates RsmA away from its mRNA targets (78).

The global decrease in siderophore production observed in the *ihfA* mutant (Figure 2) is correlated with the down-regulation of the achromobactin biosynthesis operon (*acsF-acr-acsDE-yhcA-acsCBA*) as well as the *cbrABCD* operon encoding the ABC permease for ferric achromobactin (Supplementary Table S2). At the same time, the *fct-cbsCEBAP* and *cbsH-ybdZ-cbsF* operons responsible for biosynthesis of the second siderophore, chrysobactin, are up-regulated in the *ihfA* mutant (Supplementary Table S2). These results suggest that achromobactin is probably better detected than chrysobactin under the growth conditions on CAS agar plate (Figure 2). Different transcriptional signatures for these two siderophores were already observed in response to various stress conditions (3). This may explain the rationale of producing two siderophores that may be required at different stages of infection.

Other genes related to virulence are affected in the *ihfA* mutant and contribute to its reduced pathogenic potential. Notably, expression of the *hrp* genes encoding type III secretion system and its effectors DspE, HrpN and HrpW, which suppress plant immunity and promote pathogenesis, are down-regulated (Supplementary Table S2). In agreement with these findings, it was shown that IHF is required for RpoN-dependent expression of *hrpL* gene encoding HrpL, the sigma factor coordinating the expression of the *hrp* genes in *Pseudomonas syringae* and *Erwinia amylovora* (33,79).

IHF switches the orientation preferences of transcribed genes

We observed that lack of IHF heterodimer in cells alters the preference for spatial orientation of the transcribed genes, especially under conditions of DNA relaxation. While this local effect of IHF requires further investigation, we note that it constitutes a novel and original mechanism in DNA supercoiling-dependent regulation of transcription. Analyses of previously published microarray data (11) show that H-NS does not favour any orientation, whereas FIS only slightly favours convergent genes in a relaxed chromosome (Supplementary Figure S2 in Supplementary Materials). This moderate effect of FIS compared to IHF might be related to the difference in the extent of bending ($\sim$45° for FIS and $\sim$180° for IHF) induced on binding the DNA. However, FIS constrains right-handed toroidal coils activating promoters that require high negative superhelicity (80) whereas binding of IHF constrains little, if any negative superhelicity (15,81) suggesting that IHF preferentially binds relaxed or slightly positively supercoiled DNA loops. This latter preference is consistent with two other observations. First, it was shown that IHF preferentially binds at the 3′ ends of transcription units (24) which accumulate positive superhelicity due to transcription-coupled supercoil diffusion (47,82). Second, while IHF, alike the structurally related NAP HU, untwists the DNA by proline intercalation, the net untwisting is significantly less for IHF consistent with a planar DNA bend (81,83). Furthermore, since divergent transcription is expected to increase negative superhelicity in between the genes, whereas the opposite is true for convergently organised transcription units (47,82), the former might be especially sensitive to DNA relaxation thus favouring IHF binding under this regimen. Since IHF binds DNA using both direct and indirect readout (66) stabilising various 3D structures (22), modulation of its binding by changing supercoil dynamics resulting from adjacent transcription units may lead to profound changes in the organisation of nucleoprotein complexes and depending on torsional stress, distinctly favour writhe deformations at the expense of twist. These latter can in turn favour or inhibit the formation of twist-induced DNA denaturation bubbles facilitating transcription initiation, as well as other competing structural transitions (65) and thereby affect convergent and divergent transcription units in different manner. The observed modification of leading/lagging strand utilisation further suggests that this interplay between IHF and DNA supercoils may not be limited to those generated by and affecting transcription, but also related to the replication machinery.

Lack of IHF impairs the response of CODOs

Our transcriptome analyses suggest a massive reorganization of the genomic expression patterns induced by *ihfA* mutation in *D. dadantii* cells, especially under conditions of DNA relaxation induced by novobiocin addition. DNA relaxation in *ihfA* mutant background makes the genomic expression pattern extending in both directions from OriC and Ter more uniform compared to the wild-type (Figure 11B), highlighting an asymmetry in relative activities of the chromosomal Ori and Ter ends. On the other hand, the comparison of the wild-type and *ihfA* mutant cells shows a conspicuous difference between the right and left chromosomal arms which again, is augmented under conditions of DNA relaxation. This differential regulatory effect on chromosomal arms is reminiscent of the observed spatial organization of transcriptional regulatory networks along the replichores in *E. coli* (84,85). Thus, the regulatory impacts of IHF and DNA supercoiling appear organized along the orthogonal axes (respectively along the OriC – Ter axis, and the lateral axis) of the chromosome.

Our previous finding that the *D. dadantii* major virulence and adaptation genes demonstrate a pattern of expression that is by and large, congruent with that of the CODOs harbouring them (12), suggested that the distinct expression of CODOs under various growth conditions provides a *bona fide* mechanism underlying the coordinated genetic response of the cells to environmental stress (11). This response appears impaired in *ihfA* mutant cells. For example, the CODO d7 encodes the motility and chemotaxis functions required for the colonization of the apoplast. These functions are repressed by novobiocin treatment independent of the growth phase in the absence, but not in the presence, of the IHF heterodimer (Figure 11B, compare the two inner rings with the two following ones). The CODO d6L, harbouring several virulence traits including type I and III secretion systems and plant wall-degrading enzymes (proteases and xylanase) is up-regulated in wild-type cells compared to the *ihfA* mutant (i.e. activated by IHF) in condition of DNA relaxation, albeit to different extent depending on the growth phase (Figure 11A, third and fourth rings from inside). Correspondingly, it is also repressed by DNA relaxation in *ihfA* mutant but not in the WT cells (Figure 11B, compare the second and fourth rings from inside), in stationary phase, consistent with the impairing of the associated functions in the mutant strain (Figure 2). It is noteworthy that, in the *ihfA* mutant, we observed alterations of the secretion systems underpinning the bacterial pathogenic growth, as well as the genes involved in flagellar assembly and genes of numerous membrane-anchored proteins. During the process of transcription and co-translational export, the loops of chromosomal DNA encoding the inner membrane and/or secreted proteins become transiently anchored to the plasma membrane, providing expansion forces that affect the nucleoid structure (86). We surmise that down-regulation of the corresponding genes in *ihfA* mutant may be concomitant to a profound modification of the nucleoid configuration, which might underpin the spatial organisation of expression along CODOs.

Taken together, the transcriptome analysis not only allowed us to identify gross genome-wide differences between

the responses of the wild-type and *ihfA* cells consistent with the observed general effect on virulence functions, but also to distinguish global and local effects related to the mechanism of action of the IHF heterodimer. We propose that IHF acts as a multi-scale architectural protein with a multifaceted regulatory effect. First, at the kilobase scale of topological domains, it relays the effect of DNA supercoiling in a strongly gene orientation-dependent manner. Second, at the megabase-scale of macrodomains, it acts as a 'transcriptional domainin' protein defining the boundaries of the transcriptional supercoiling response and preventing its expansion across the CODOs and thus preventing aberrant expression of different virulence genes. Third, IHF heterodimer globally affects the preference for leading versus lagging strand utilization and thus determines the default setting for the directionality of transcription in the genome. We propose that in *ihfA* mutant this systemic effect of the IHF heterodimer on local and global transcription required for faithful operation of the virulence program is lost, leading to abrogation of bacterial pathogenicity.Altogether, this study shows that the integrated regulatory impacts of the NAPs and DNA supercoiling play a pivotal role in bacterial gene expression, and their exploration constitutes a promising avenue for future research.

DATA AVAILABILITY

RNA-Seq data have been deposited at ArrayExpress repositories E-MTAB-7650 (WT strain) and E-MTAB-9025 (*ihfA* strain).

SUPPLEMENTARY DATA

Supplementary Data are available at NAR Online.

ACKNOWLEDGEMENTS

The authors thank Corentin Schotte, Florelle Deboudard, Elodie Kenck, Camille Villard for technical support and Hubert Charles for helpful discussions.

FUNDING

INSA grant (to G.M.) as visiting researcher; R.F. was funded by a research allocation from the French Ministry; INSA Lyon grants [BQR 2016 to S.M.]; IXXI; Agence Nationale de la Recherche [ANR-18-CE45-0006-01 to S.M.]; Breakthrough Phytobiome IDEX LYON project, Université de Lyon Programme d'investissements d'Avenir [ANR16-IDEX-0005]; Centre National de la Recherche Scientifique [to S.R., F.H., W.N., S.M.]; Université de Lyon [to S.R., F.H., W.N., S.M.]. Funding for open access charge: CNRS recurrent funding.
Conflict of interest statement. None declared.

REFERENCES

1. Glasner,J.D., Yang,C.H., Reverchon,S., Hugouvieux-Cotte-Pattat,N., Condemine,G., Bohin,J.P., Van Gijsegem,F., Yang,S., Franza,T., Expert,D. *et al.* (2011) Genome sequence of the plant-pathogenic bacterium *Dickeya dadantii* 3937. *J. Bacteriol.*, **193**, 2076–2077.
2. Reverchon,S., Muskhelisvili,G. and Nasser,W. (2016) Virulence program of a bacterial plant pathogen: the *Dickeya* model. *Prog. Mol. Biol. Transl. Sci.*, **142**, 51–92.
3. Jiang,X., Zghidi-Abouzid,O., Oger-Desfeux,C., Hommais,F., Greliche,N., Muskhelishvili,G., Nasser,W. and Reverchon,S. (2016) Global transcriptional response of *Dickeya dadantii* to environmental stimuli relevant to the plant infection. *Environ. Microbiol.*, **18**, 3651–3672.
4. Lautier,T., Blot,N., Muskhelishvili,G. and Nasser,W. (2007) Integration of two essential virulence modulating signals at the *Erwinia chrysanthemi pel* gene promoters: a role for Fis in the growth-phase regulation. *Mol. Microbiol.*, **66**, 1491–1505.
5. Sepulchre,J.A., Reverchon,S. and Nasser,W. (2007) Modeling the onset of virulence in a pectinolytic bacterium. *J. Theor. Biol.*, **244**, 239–257.
6. Hommais,F., Oger-Desfeux,C., Van Gijsegem,F., Castang,S., Ligori,S., Expert,D., Nasser,W. and Reverchon,S. (2008) PecS is a global regulator of the symptomatic phase in the phytopathogenic bacterium *Erwinia chrysanthemi* 3937. *J. Bacteriol.*, **190**, 7508–7522.
7. Kepseu,W.D., Sepulchre,J.A., Reverchon,S. and Nasser,W. (2010) Toward a quantitative modeling of the synthesis of the pectate lyases, essential virulence factors in *Dickeya dadantii*. *J. Biol. Chem.*, **285**, 28565–28576.
8. Reverchon,S. and Nasser,W. (2013) *Dickeya* ecology, environment sensing and regulation of virulence programme. *Environ. Microbiol. Rep.*, **5**, 622–636.
9. Dorman,C.J. and Deighan,P. (2003) Regulation of gene expression by histone-like proteins in bacteria. *Curr. Opin. Genet. Dev.*, **13**, 179–184.
10. Travers,A. and Muskhelishvili,G. (2005) DNA supercoiling - a global transcriptional regulator for enterobacterial growth? *Nat. Rev. Microbiol.*, **3**, 157–169.
11. Jiang,X., Sobetzko,P., Nasser,W., Reverchon,S. and Muskhelishvili,G. (2015) Chromosomal 'stress-response' domains govern the spatiotemporal expression of the bacterial virulence program. *mBio*, **6**, e00353-15.
12. Meyer,S., Reverchon,S., Nasser,W. and Muskhelishvili,G. (2018) Chromosomal organization of transcription: in a nutshell. *Curr. Genet.*, **64**, 555–565.
13. Muskhelishvili,G., Forquet,R., Reverchon,S., Meyer,S. and Nasser,W. (2019) Coherent domains of transcription coordinate gene expression during bacterial growth and adaptation. *Microorganisms*, **7**, 694.
14. Ouafa,Z.A., Reverchon,S., Lautier,T., Muskhelishvili,G. and Nasser,W. (2012) The nucleoid-associated proteins H-NS and FIS modulate the DNA supercoiling response of the *pel* genes, the major virulence factors in the plant pathogen bacterium *Dickeya dadantii*. *Nucleic Acids Res.*, **40**, 4306–4319.
15. Rice,P.A., Yang,S., Mizuuchi,K. and Nash,H.A. (1996) Crystal structure of an IHF-DNA complex: a protein-induced DNA U-turn. *Cell*, **87**, 1295–1306.
16. Bushman,W., Thompson,J.F., Vargas,L. and Landy,A. (1985) Control of directionality in lambda site specific recombination. *Science*, **230**, 906–911.
17. Makris,J.C., Nordmann,P.L. and Reznikoff,W.S. (1990) Integration host factor plays a role in IS50 and Tn5 transposition. *J. Bacteriol.*, **172**, 1368–1373.
18. Goosen,N. and van de Putte,P. (1995) The regulation of transcription initiation by integration host factor. *Mol. Microbiol.*, **16**, 1–7.
19. Ryan,V.T., Grimwade,J.E., Nievera,C.J. and Leonard,A.C. (2002) IHF and HU stimulate assembly of pre-replication complexes at *Escherichia coli oriC* by two different mechanisms. *Mol. Microbiol.*, **46**, 113–124.
20. Harshey,R.M. (2014) Transposable Phage Mu. *Microbiol. Spectr*, **2**, doi:10.1128/microbiolspec.MDNA3-0007-2014.
21. Kasho,K., Fujimitsu,K., Matoba,T., Oshima,T. and Katayama,T. (2014) Timely binding of IHF and Fis to DARS2 regulates ATP-DnaA production and replication initiation. *Nucleic Acids Res.*, **42**, 13134–13149.
22. Lee,S.Y., Lim,C.J., Droge,P. and Yan,J. (2015) Regulation of bacterial DNA packaging in early stationary phase by competitive DNA binding of Dps and IHF. *Sci. Rep.*, **5**, 18146.
23. Jia,J., King,J.E., Goldrick,M.C., Aldawood,E. and Roberts,I.S. (2017) Three tandem promoters, together with IHF, regulate growth

phase dependent expression of the *Escherichia coli kps* capsule gene cluster. *Sci. Rep.*, **7**, 17924.
24. Boccard,F. and Prentki,P. (1993) Specific interaction of IHF with RIBs, a class of bacterial repetitive DNA elements located at the 3′ end of transcription units. *EMBO J.*, **12**, 5019–5027.
25. Blot,N., Mavathur,R., Geertz,M., Travers,A. and Muskhelishvili,G. (2006) Homeostatic regulation of supercoiling sensitivity coordinates transcription of the bacterial genome. *EMBO Rep.*, **7**, 710–715.
26. Azam,T.A. and Ishihama,A. (1999) Twelve species of the nucleoid-associated protein from *Escherichia coli*. Sequence recognition specificity and DNA binding affinity. *J. Biol. Chem.*, **274**, 33105–33113.
27. Haverkorn van Rijsewijk,B.R.B., Nanchen,A., Nallet,S., Kleijn Roelco,J. and Uwe,S. (2011) Large-scale 13C-flux analysis reveals distinct transcriptional control of respiratory and fermentative metabolism in *Escherichia coli*. *Mol Syst Biol.*, **7**, 477.
28. Prieto,A.I., Kahramanoglou,C., Ali,R.M., Fraser,G.M., Seshasayee,A.S. and Luscombe,N.M. (2012) Genomic analysis of DNA binding and gene regulation by homologous nucleoid-associated proteins IHF and HU in *Escherichia coli* K12. *Nucleic Acids Res.*, **40**, 3524–3537.
29. Mangan,M.W., Lucchini,S., Danino,V., Croinin,T.O., Hinton,J.C. and Dorman,C.J. (2006) The integration host factor (IHF) integrates stationary-phase and virulence gene expression in *Salmonella enterica* serovar *Typhimurium*. *Mol. Microbiol.*, **59**, 1831–1847.
30. Leite,B., Werle,C.H., Carmo,C.P.D., Nóbrega,D.B., Milanez,G.P., Culler,H.F., Sircili,M.P., Alvarez-Martinez,C.E. and Marcelo,B. (2017) Integration host factor is important for biofilm formation by *Salmonella enterica Enteritidis*. *Pathog Dis.*, **75**, ftx074.
31. Stonehouse,E., Kovacikova,G., Taylor,R.K. and Skorupski,K. (2008) Integration host factor positively regulates virulence gene expression in *Vibrio cholerae*. *J. Bacteriol.*, **190**, 4736–4748.
32. Pan,J., Zhao,M., Huang,Y., Li,J., Liu,X., Ren,Z., Kan,B. and Liang,W. (2018) Integration host factor modulates the expression and function of T6SS2 in *Vibrio fluvialis*. *Front Microbiol*, **9**, 962.
33. Lee,J.H. and Zhao,Y. (2016) Integration host factor is required for RpoN-Dependent *hrpL* gene expression and controls motility by positively regulating *rsmB* sRNA in *Erwinia amylovora*. *Phytopathology*, **106**, 29–36.
34. Chen,X., Yu,C., Li,S., Li,X. and Liu,Q. (2019) Integration host factor is essential for biofilm formation, extracellular enzyme, zeamine production, and virulence in *Dickeya zeae*. *Mol. Plant Microbe Interact.*, **32**, 325–335.
35. Silva-Rocha,R., Chavarria,M., Kleijn,R.J., Sauer,U. and de Lorenzo,V. (2013) The IHF regulon of exponentially growing *Pseudomonas putida* cells. *Environ. Microbiol.*, **15**, 49–63.
36. Douillie,A., Toussaint,A. and Faelen,M. (1994) Identification of the integration host factor genes of *Erwinia chrysanthemi* 3937. *Biochimie*, **76**, 1055–1062.
37. Prigent-Combaret,C., Zghidi-Abouzid,O., Effantin,G., Lejeune,P., Reverchon,S. and Nasser,W. (2012) The nucleoid-associated protein Fis directly modulates the synthesis of cellulose, an essential component of pellicle-biofilms in the phytopathogenic bacterium *Dickeya dadantii*. *Mol. Microbiol.*, **86**, 172–186.
38. Resibois,A., Colet,M., Faelen,M., Schoonejans,E. and Toussaint,A. (1984) Phi-Ec2, a new generalized transducing phage of *Erwinia chrysanthemi*. *Virology*, **137**, 102–112.
39. Miller,J.H. (1972) *Experiments in Molecular Genetics*. NY.
40. Teather,R.M. and Wood,P.J. (1982) Use of Congo red-polysaccharide interactions in enumeration and characterization of cellulolytic bacteria from the bovine rumen. *Appl. Environ. Microbiol.*, **43**, 777–780.
41. Reverchon,S., Nasser,W. and Robert-Baudouy,J. (1994) *pecS*: a locus controlling pectinase, cellulase and blue pigment production in *Erwinia chrysanthemi*. *Mol. Microbiol.*, **11**, 1127–1139.
42. Schwyn,B. and Neilands,J.B. (1987) Universal chemical assay for the detection and determination of siderophores. *Anal. Biochem.*, **160**, 47–56.
43. Moran,F., Nasuno,S. and Starr,M.P. (1968) Extracellular and intracellular polygalacturonic acid trans-eliminases of *Erwinia carotovora*. *Arch. Biochem. Biophys.*, **123**, 298–306.
44. Lautier,T. and Nasser,W. (2007) The DNA nucleoid-associated protein Fis co-ordinates the expression of the main virulence genes in the phytopathogenic bacterium *Erwinia chrysanthemi*. *Mol. Microbiol.*, **66**, 1474–1490.
45. Carey,J. (1988) Gel retardation at low pH resolves trp repressor-DNA complexes for quantitative study. *Proc. Natl. Acad. Sci. U.S.A.*, **85**, 975–979.
46. Maes,M. and Messens,E. (1992) Phenol as grinding material in RNA preparations. *Nucleic Acids Res.*, **20**, 4374.
47. El Houdaigui,B., Forquet,R., Hindre,T., Schneider,D., Nasser,W., Reverchon,S. and Meyer,S. (2019) Bacterial genome architecture shapes global transcriptional regulation by DNA supercoiling. *Nucleic Acids Res.*, **47**, 5648–5657.
48. Eckweiler,D., Dudek,C.A., Hartlich,J., Brotje,D. and Jahn,D. (2018) PRODORIC2: the bacterial gene regulation database in 2018. *Nucleic Acids Res.*, **46**, D320–D326.
49. SantaLucia,J. (1998) A unified view of polymer, dumbbell, and oligonucleotide DNA nearest-neighbor thermodynamics. *Proc. Natl. Acad. Sci. U.S.A.*, **95**, 1460–1465.
50. Werner,M.H., Clore,G.M., Gronenborn,A.M. and Nash,H.A. (1994) Symmetry and asymmetry in the function of *Escherichia coli* integration host factor: implications for target identification by DNA-binding proteins. *Curr. Biol.*, **4**, 477–487.
51. Zulianello,L., de la Gorgue de Rosny,E., van Ulsen,P., van de Putte,P. and Goosen,N. (1994) The HimA and HimD subunits of integration host factor can specifically bind to DNA as homodimers. *EMBO J.*, **13**, 1534–1540.
52. Zablewska,B. and Kur,J. (1995) Mutations in HU and IHF affect bacteriophage T4 growth: HimD subunits of IHF appear to function as homodimers. *Gene*, **160**, 131–132.
53. Enard,C., Diolez,A. and Expert,D. (1988) Systemic virulence of *Erwinia chrysanthemi* 3937 requires a functional iron assimilation system. *J. Bacteriol.*, **170**, 2419–2426.
54. Dellagi,A., Segond,D., Rigault,M., Fagard,M., Simon,C., Saindrenan,P. and Expert,D. (2009) Microbial siderophores exert a subtle role in Arabidopsis during infection by manipulating the immune response and the iron status. *Plant Physiol.*, **150**, 1687–1696.
55. Shingler,V. (2011) Signal sensory systems that impact σ^{54} -dependent transcription. *FEMS Microbiol. Rev.*, **35**, 425–440.
56. Hoover,T.R., Santero,E., Porter,S. and Kustu,S. (1990) The integration host factor stimulates interaction of RNA polymerase with NifA, the transcriptional activator for nitrogen fixation operons. *Cell*, **63**, 11–22.
57. Cebolla,A., Ruiz-Berraquero,F. and Palomares,A.J. (1994) Analysis of the expression from *Rhizobium meliloti fix*-promoters in other *Rhizobium* backgrounds. *Microbiology*, **140**, 443–453.
58. Koskiniemi,S., Lamoureux,J.G., Nikolakakis,K.C., T'Kint de Roodenbeke,C., Kaplan,M.D., Low,D.A. and Hayes,C.S. (2013) Rhs proteins from diverse bacteria mediate intercellular competition. *Proc. Natl Acad. Sci. U.S.A.*, **110**, 7032–7037.
59. Franza,T., Enard,C., van Gijsegem,F. and Expert,D. (1991) Genetic analysis of the *Erwinia chrysanthemi* 3937 chrysobactin iron-transport system: characterization of a gene cluster involved in uptake and biosynthetic pathways. *Mol. Microbiol.*, **5**, 1319–1329.
60. Franza,T., Mahe,B. and Expert,D. (2005) *Erwinia chrysanthemi* requires a second iron transport route dependent of the siderophore achromobactin for extracellular growth and plant infection. *Mol. Microbiol.*, **55**, 261–275.
61. Liu,L., Gueguen-Chaignon,V., Goncalves,I.R., Rascle,C., Rigault,M., Dellagi,A., Loisel,E., Poussereau,N., Rodrigue,A., Terradot,L. *et al.* (2019) A secreted metal-binding protein protects necrotrophic phytopathogens from reactive oxygen species. *Nat. Commun.*, **10**, 4853.
62. Reverchon,S., Rouanet,C., Expert,D. and Nasser,W. (2002) Characterization of indigoidine biosynthetic genes in *Erwinia chrysanthemi* and role of this blue pigment in pathogenicity. *J. Bacteriol.*, **184**, 654–665.
63. Ellenberger,T. and Landy,A. (1997) A good turn for DNA: the structure of integration host factor bound to DNA. *Structure*, **5**, 153–157.
64. Marr,C., Geertz,M., Hutt,M.T. and Muskhelishvili,G. (2008) Dissecting the logical types of network control in gene expression profiles. *BMC Syst. Biol.*, **2**, 18.
65. Sheridan,S.D., Benham,C.J. and Hatfield,G.W. (1999) Inhibition of DNA supercoiling-dependent transcriptional activation by a distant B-DNA to Z-DNA transition. *J. Biol. Chem.*, **274**, 8169–8174.

66. Travers,A. (1997) DNA-protein interactions: IHF-the master bender.*Curr. Biol.*, **7**, R252–R254.
67. Sobetzko,P., Glinkowska,M., Travers,A. and Muskhelishvili,G. (2013) DNA thermodynamic stability and supercoil dynamics determine the gene expression program during the bacterial growth cycle. *Mol. Biosyst.*, **9**, 1643–1651.
68. Travers,A. and Muskhelishvili,G. (2020) Chromosomal organization and regulation of genetic function in *Escherichia coli* integrates the DNA analog and digital information. *EcoSal Plus*, **9**, doi:10.1128/ecosalplus.ESP-0016-2019.
69. Travers,A. and Muskhelishvili,G. (2005) Bacterial chromatin. *Curr. Opin. Genet. Dev.*, **15**, 507–514.
70. Nasser,W., Faelen,M., Hugouvieux-Cotte-Pattat,N. and Reverchon,S. (2001) Role of the nucleoid-associated protein H-NS in the synthesis of virulence factors in the phytopathogenic bacterium *Erwinia chrysanthemi*. *Mol. Plant Microbe Interact.*, **14**, 10–20.
71. Antunez-Lamas,M., Cabrera-Ordonez,E., Lopez-Solanilla,E., Raposo,R., Trelles-Salazar,O., Rodriguez-Moreno,A. and Rodriguez-Palenzuela,P. (2009) Role of motility and chemotaxis in the pathogenesis of *Dickeya dadantii* 3937 (ex *Erwinia chrysanthemi* 3937). *Microbiology*, **155**, 434–442.
72. Pesavento,C. and Hengge,R. (2012) The global repressor FliZ antagonizes gene expression by sigmaS-containing RNA polymerase due to overlapping DNA binding specificity. *Nucleic Acids Res.*, **40**, 4783–4793.
73. Burdman,S., Bahar,O., Parker,J.K. and De La Fuente,L. (2011) Involvement of type IV Pili in pathogenicity of plant pathogenic bacteria. *Genes*, **2**, 706–735.
74. Nasser,W. and Reverchon,S. (2002) H-NS-dependent activation of pectate lyases synthesis in the phytopathogenic bacterium *Erwinia chrysanthemi* is mediated by the PecT repressor. *Mol. Microbiol.*, **43**, 733–748.
75. Duprey,A., Muskhelishvili,G., Reverchon,S. and Nasser,W. (2016) Temporal control of *Dickeya dadantii* main virulence gene expression by growth phase-dependent alteration of regulatory nucleoprotein complexes. *Biochim. Biophys. Acta*, **1859**, 1470–1480.
76. Reverchon,S., Van Gijsegem,F., Effantin,G., Zghidi-Abouzid,O. and Nasser,W. (2010) Systematic targeted mutagenesis of the MarR/SlyA family members of *Dickeya dadantii* 3937 reveals a role for MfbR in the modulation of virulence gene expression in response to acidic pH. *Mol. Microbiol.*, **78**, 1018–1037.
77. Cui,Y., Chatterjee,A., Liu,Y., Dumenyo,C.K. and Chatterjee,A.K. (1995) Identification of a global repressor gene, *rsmA*, of *Erwinia carotovora* subsp. *carotovora* that controls extracellular enzymes, N-(3-oxohexanoyl)-L-homoserine lactone, and pathogenicity in soft-rotting *Erwinia* spp. *J. Bacteriol.*, **177**, 5108–5115.
78. Vakulskas,C.A., Potts,A.H., Babitzke,P., Ahmer,B.M. and Romeo,T. (2015) Regulation of bacterial virulence by Csr (Rsm) systems. *Microbiol. Mol. Biol. Rev.*, **79**, 193–224.
79. Waite,C., Schumacher,J., Jovanovic,M., Bennett,M. and Buck,M. (2017) Negative autogenous control of the master type III secretion system regulator HrpL in Pseudomonas syringae. *mBio*, **8**, e02273-16.
80. Maurer,S., Fritz,J., Muskhelishvili,G. and Travers,A. (2006) RNA polymerase and an activator form discrete subcomplexes in a transcription initiation complex. *EMBO J.*, **25**, 3784–3790.
81. Swinger,K.K. and Rice,P.A. (2004) IHF and HU: flexible architects of bent DNA. *Curr. Opin. Struct. Biol.*, **14**, 28–35.
82. Sobetzko,P. (2016) Transcription-coupled DNA supercoiling dictates the chromosomal arrangement of bacterial genes. *Nucleic Acids Res.*, **44**, 1514–1524.
83. Swinger,K.K., Lemberg,K.M., Zhang,Y. and Rice,P.A. (2003) Flexible DNA bending in HU-DNA cocrystal structures. *EMBO J.*, **22**, 3749–3760.
84. Sobetzko,P., Travers,A. and Muskhelishvili,G. (2012) Gene order and chromosome dynamics coordinate spatiotemporal gene expression during the bacterial growth cycle. *Proc. Natl Acad. Sci. U.S.A.*, **109**, E42–E50.
85. Kosmidis,K., Jablonski,K.P., Muskhelishvili,G. and Hutt,M.T. (2020) Chromosomal origin of replication coordinates logically distinct types of bacterial genetic regulation. *NPJ Syst. Biol. Appl.*, **6**, 5.
86. Woldringh,C.L. (2002) The role of co-transcriptional translation and protein translocation (transertion) in bacterial chromosome segregation. *Mol. Microbiol.*, **45**, 17–29.